OPEN ACCESS
JOURNAL OF ADVANCED DIELECTRICS
Vol. 13, No. 5 (2023) 2350012 (8 pages)

DOI: 10.1142/S2010135X23500121

High piezoelectricity performance in PSBZT ceramic for ultrasonic transducer

Shengpeng Han[*], Guicheng Jiang[*,¶,††], Yan Zhu[*], Yingchun Liu[*], Hongjun Zhang[*], Lang Bian[*,‖,††], Danqing Liu[†], Ye Sun[*], Limei Zheng[‡], Bin Yang[*,**,††] and Wenwu Cao[§]

[*]*School of Instrumentation Science and Engineering, Harbin Institute of Technology Harbin 150080, P. R. China*

[†]*School of Chemical and Environmental Engineering, Harbin University of Science and Technology Harbin 150040, P. R. China*

[‡]*School of Physics, Shandong University, Jinan 250100, P. R. China*

[§]*Materials Research Institute, The Pennsylvania State University, University Park Pennsylvania 16802, USA*

[¶]gjiang@hit.edu.cn
[‖]bianlang@hit.edu.cn
[**]binyang@hit.edu.cn

Received 27 February 2023; Revised 24 March 2023; Accepted 3 April 2023; Published 6 May 2023

Lead zirconate titanate (PZT) ceramics possess great potential for practical applications and thus improving their piezoelectric properties is crucial. $Pb_{0.99-x}Sm_{0.01}Ba_xZr_{0.53}Ti_{0.47}O_3$ (PSBZT) ceramics with high Curie temperature and excellent piezoelectric properties were fabricated via a conventional solid-state method, and the effect of Ba^{2+} doping on the structural, dielectric, piezoelectric and ferroelectric properties was studied in detail. It is shown that doping of Ba^{2+} significantly enhanced the piezoelectric properties of PSZT, the maximum d_{33}~533 pC/N and T_c ~361°C at $x = 0.02$ were acquired. Furthermore, PSZT and PSBZT ceramics were used to prepare single element ultrasonic transducers, and their performance were compared and evaluated. The results demonstrate that the PSBZT ceramic-based transducer possesses better sensitivity and bandwidth than the PSZT ceramic-based transducer.

Keywords: PSBZT; piezoelectricity; ultrasonic transducer.

1. Introduction

Piezoelectric materials achieve the electromechanical conversion between electrical energy and mechanical energy and vice-versa.[1–3] Various kinds of piezoelectric components, such as ultrasound transducers, pressure sensors, piezoelectric actuators and filters, are widely used in a variety of military and civilian applications, including aircraft industry, medical devices, ocean exploration, petroleum exploration and security systems.[4–6] As the most widely used piezoelectric ceramic material, PZT-based ceramics have attracted much attention due to their higher Curie temperature and stable piezoelectric properties.[7–10] Therefore, the performance optimization of PZT-based ceramics has been one of the hot topics of research.[11–14]

In addition to the phase structure modulation, donor doping is also a process method that can also be used to effectively improve the piezoelectric properties of ceramics. Lead vacancies are generated in ceramics by substitution of highly valent ions (such as Nb^{5+}, La^{3+}, Nd^{3+}, Sm^{3+}, etc.), which accelerate the motion of the domain wall and therefore improve the piezoelectric properties.[15] Among these metal ions, Sm^{3+} has recently received extensive attention as a result of the unexpected high piezoelectric response in lead-based ceramics. Li *et al*. have successfully prepared the PMN-PT piezoelectric ceramics by doping Sm^{3+} at the A-site. The ceramic possesses giant piezoelectric coefficients d_{33} of 1510 pC/N, dielectric permittivity $\varepsilon_{33}/\varepsilon_0$ of 13,000 and Curie temperature of 89°C.[16] They stated that the major reason for the remarkable enhancement of piezoelectric and dielectric properties is the construction of the local structural heterogeneity, which flattens the average free energy curve of the system. Similarly, Seshadri *et al*. reported $Pb_{0.97}Sm_{0.02}Zr_xTi_{1-x}O_3$ (PSZT) ceramics, which have high temperature piezoelectric coefficients.[17] Obviously, the construction of local structural heterogeneity by doping Sm^{3+} is an effective means to improve the electromechanical properties of ceramics.

Apart from high-valent metal ions, other valence metal ions are also employed to improve the performance of PZT ceramic systems, such as replacing Pb^{2+} cations with Ba^{2+} to form a Pb_{1-x} $Ba_xZr_{1-y}Ti_yO_3$ (PBZT) ceramic system. The Ba-substitution does not generate vacancies due to the equivalence substitution. However, adding Ba^{2+} to the A-sites of the ABO_3 perovskite structure of PZT ceramics improves both the ferroelectric and piezoelectric properties, which

[††]Corresponding authors.

could be attributed to structural defects created by the difference of Pb and Ba ions. Ikeda reported the results of the first detailed study on PBZT systems.[18] In his work, Ikeda investigated the crystal structure and dielectric properties of a series of constituents and identified the phase diagram of the entire system according to the results of dielectric permittivity and X-ray diffraction (XRD) measurement. Recently, Xu *et al*. prepared high-transparent electro-optic ceramics $Pb_{0.91-x}Ba_xLa_{0.09}(Zr_{0.65}Ti_{0.35})_{0.9775}O_3$ doped with different amounts of Ba by hot-pressing sintering process, and found that the doping of Ba^{2+} ions would weaken the ferroelectric hysteresis.[19]

In this paper, the co-doping of rare earth ions and equivalent ions will be used to optimize the performance of PZT-based ceramics. One of the main focuses of this work is to study the effect of Ba^{2+} doping on the dielectric and piezoelectric properties of PSZT ceramics in detail. Moreover, ultrasonic transducers were prepared by PSZT and PSBZT ceramics. The insertion loss (IL) and bandwidth of these ultrasonic transducers were measured and compared.

2. Experimental Procedure

$Pb_{0.99-x}Sm_{0.01}Ba_xZr_{0.53}Ti_{0.47}O_3$ (PSBZT) ceramics with x = 0, 0.01, 0.02, 0.03, 0.04, 0.05 were fabricated via a conventional solid-state method. PbO (99.9%), ZrO_2 (99.99%), TiO_2 (99%), Sm_2O_3 (99.99%) and $BaCO_3$ (99%) were used as the starting materials. All the starting materials were weighed based on the stoichiometric ratio and then milled in the alcohol with zirconia balls for 12 h. The resulting mixture was calcined at 800°C for 3 h and the calcined powder was milled again. The binder of 7 wt.% polyvinyl alcohol (PVA) was added to the powder and compressed into green disks with the diameter of 13 mm. The prepared disks were binder-burned out at 550°C to exclude the PVA, then inserted in sacrificial powder and sintered at 1220°C for 2 h.

The crystalline phases of the ceramics were evidenced by XRD (D/max 2400, Rigaku Corporation, Tokyo, Japan). The fractured surface micromorphology of the sintered samples was determined by the scanning electron microscopy (SEM, Quanta 200FEG, FEI, USA). The samples were screen-printed with silver electrodes on both the surfaces and then were fired at 600°C for 30 min. Dielectric-temperature curves were obtained by an LCR meter (Agilent E4980A, Agilent Technologies, CA, USA). For piezoelectric properties, the ceramics were polarized in a silicone oil bath at room temperature (about 30°C) under a direct current (DC) field of 3 kV/mm^{-1} for 30 min. The piezoelectric coefficient d_{33} was measured by a quasi-static meter (ZJ-4A, Institute of Acoustics, Beijing, China). The ferroelectric hysteresis loops of the ceramic samples were measured by the ferroelectric test system.

The transducer performance was characterized by Pulse-echo response measurements. An electrical pulse was supplied to the transducer with an ultrasonic pulser/receiver (5073PR, Olympus, Japan) at a repetition rate of 500 Hz and a damping of 50 Ω. The energy was set to 2 μJ. The time domain echo response was captured and displayed on an oscilloscope (DPO4104, Tektronix, USA). The spectrum of the pulse-echo waveform can be obtained by the fast Fourier transform (FFT). The center frequency and bandwidth of the transducer can then be calculated from the spectrum. Sensitivity is the ability of an ultrasound transducer to detect the penetration of ultrasound waves in tissue, and is described by the bidirectional IL, which is the ratio of the output voltage of the transducer to the drive voltage. The two-way IL is calculated by Eq. (1). The Pulse-echo response measurements were as follows:

$$\mathrm{IL} = 20\log\left(\frac{V_O}{V_i}\right), \tag{1}$$

where V_O and V_i are the output and input voltages of the transducer, respectively.[20]

3. Results and Discussion

Figure 1(a) shows the XRD patterns of the PSBZT samples with various Ba contents. The pure perovskite structure without obvious secondary peaks can be seen for all ceramic samples, which means Ba doping can develop homogeneous solid solutions by substituting cations at the A site. The schematic diagram is shown in Figs. 1(c) and 1(d). Figure 1(b) displays the enlarged XRD patterns around $2\theta \approx 45°$, and the diffraction peaks gradually shift towards low angle, implying the introduction of Ba ions that lead to the increase in PSZT lattice, which is related to the larger ionic radius of Ba^{2+}. The diffraction line splits into doublets, (002) and (200), which are apparent at an angle of $2\theta \approx 45°$ in these XRD patterns. This result implies that all specimens are in tetragonal crystal structure at the room temperature.[21]

The micrographs of the fracture surface of PSBZT ceramics are shown in Fig. 2. The SEM images demonstrate that all the PSBZT samples possess dense microstructure, with well-grown grain and pore-free, which is necessary for the ceramics to own superior mechanical performance. It is also observed that the PSBZT system has an average grain size of 6–8 μm, indicating that the variation of Ba content in the PSBZT system has a negligible effect on the grain size of the ceramics.

Figure 3 depicts the relative dielectric permittivity (ε_r) versus temperature curves of the PSBZT samples, which were measured at three test frequency conditions (1, 10 and 100 kHz). It is observed that the Curie temperature (T_c) of the PSBZT specimens move toward lower temperatures with the increasing of the Ba^{2+} content. They occur at $T_c \approx 376.0$, 368.2, 361.0, 353.2, 345.9 and 344.4°C, respectively measured at 1 kHz, which indicates the ferroelectric–paraelectric phase transition become easier, and the energy requirement for ferroelectric–paraelectric phase transition decreased.[22] The detailed dielectric properties of PSBZT ceramics are

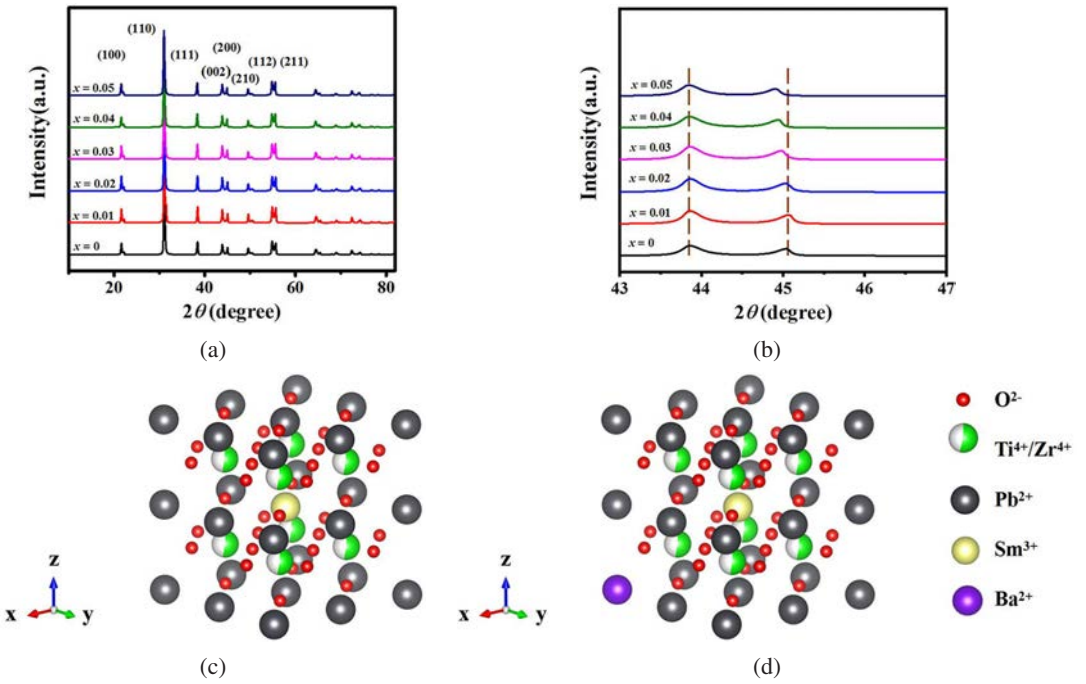

Fig. 1. (a) Room-temperature XRD patterns of PSBZT samples with different Ba content, (b) Fine-scan patterns focusing on 2θ of 43°– 47°, (c) Schematic illustration of the PSZT ceramics and (d) Schematic illustration of the PSBZT ceramics.

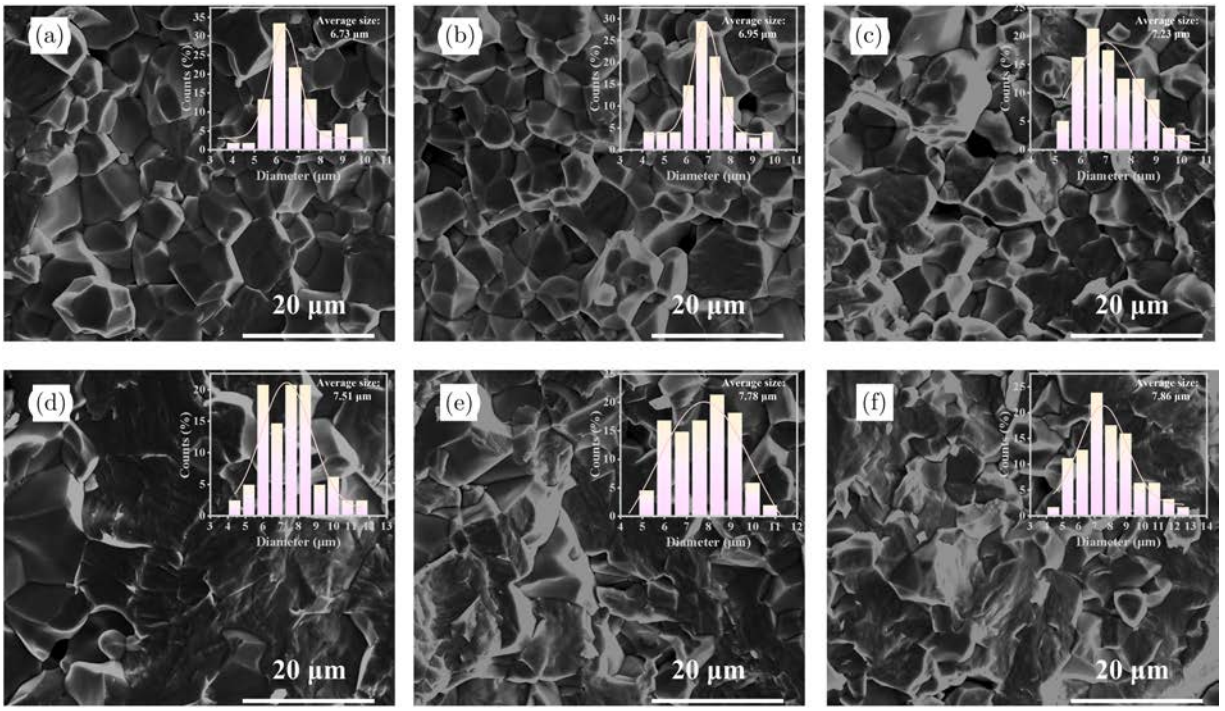

Fig. 2. The fractured surface SEM images of PSBZT ceramics with different Ba content: (a) $x = 0$, (b) $x = 0.01$, (c) $x = 0.02$, (d) $x = 0.03$, (e) $x = 0.04$ and (f) $x = 0.05$.

listed in Table 1. Compared with the undoped sample, the ε_r for the doped Ba^{2+} sample significantly increased, which would be beneficial for the acquisition of high piezoelectric property.

Figure 4(a) presents the hysteresis loops of PSBZT ceramics with different amount of Ba^{2+} at room temperature, which demonstrate perfect saturation in the applied electric field. Figure 4(b) shows the variation of coercive field

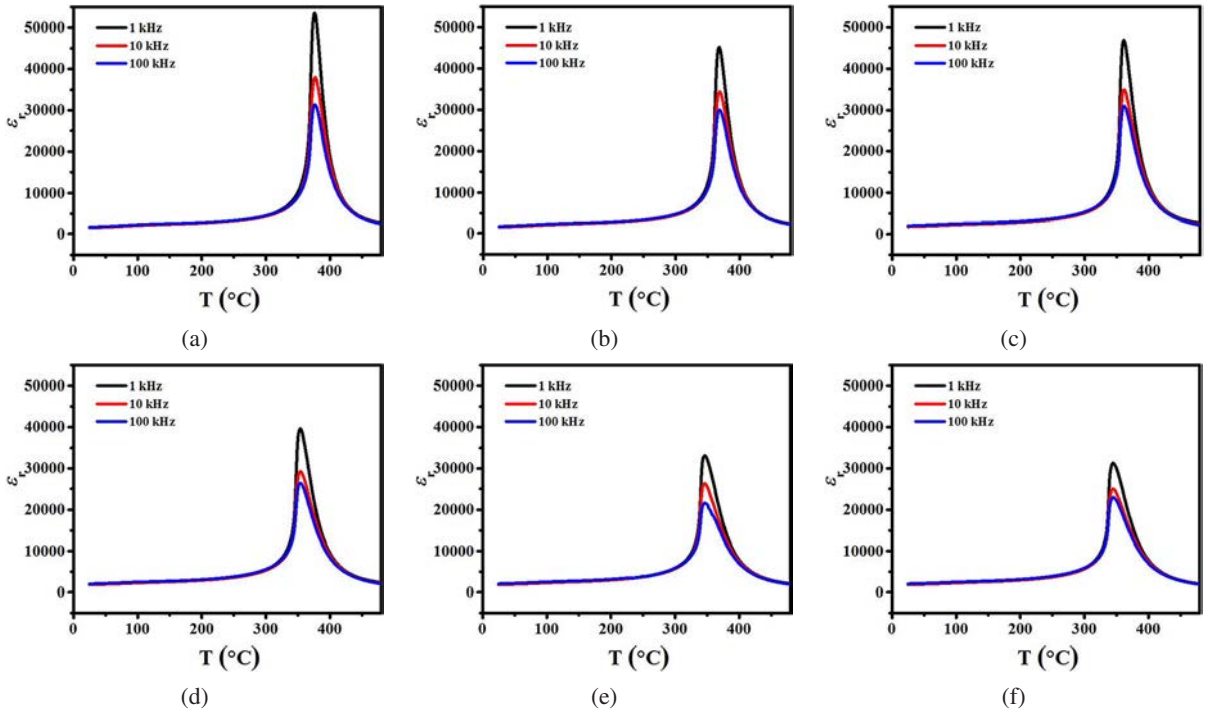

Fig. 3. The relative dielectric constant (ε_r) dependence on temperature observed in PSBZT ceramics with (a) $x = 0$, (b) $x = 0.01$, (c) $x = 0.02$, (d) $x = 0.03$, (e) $x = 0.04$ and (f) $x = 0.05$.

Table 1. Dielectric properties at 1 kHz.

Ba^{2+} contents	T_c (°C)	ε_r	tanδ
0	376.0	1512	0.015
0.01	368.2	1519	0.015
0.02	361.0	1850	0.014
0.03	353.2	1861	0.014
0.04	345.9	1868	0.014
0.05	344.4	1880	0.015

(E_c) and remanent polarization (P_r) for all samples. With the increase in Ba^{2+} content, the E_c remains essentially the same and the P_r decreases from 39.11 μC/cm^2 to 36.17 μC/cm^2. It is considered that these phenomena are caused by the strong decoupling ability of BO_6 when Ba^{2+} is substituted for Pb^{2+}, which destroys the development of long-range ferroelectric order, thus resulting in the formation of numerous nanopolar domains. Additionally, these phenomena may also be due to the replacement of Pb sites with relatively nonvolatile Ba in the composition, thus reducing the lead vacancies.[23]

Figure 5(a) illustrates the piezoelectric properties of PSBZT ceramics with the variation of Ba content. It is evident that the piezoelectric coefficient d_{33} rises from 462 pC/N to 533 pC/N at $x = 0$–0.02 and then reduces with increasing Ba^{2+} content. The high piezoelectric coefficients are related to their high dielectric constants as evidenced by the formula $d_{33} = 2Q_{33}P_r\varepsilon_{33}$.[13] In the PSBZT ceramics, the enhancement

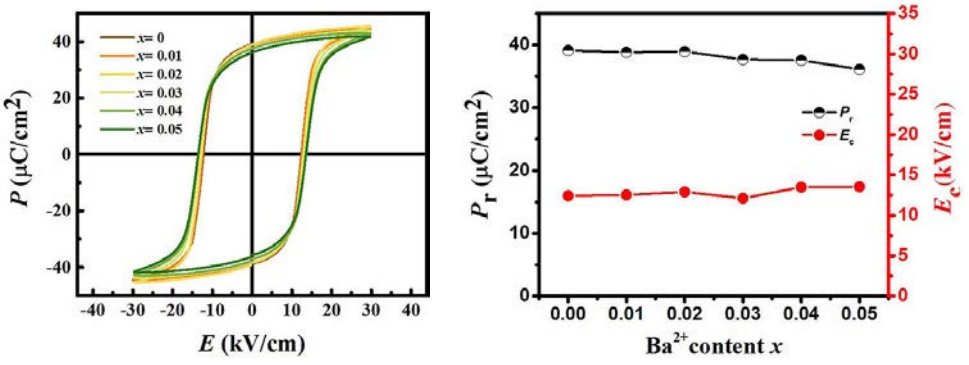

Fig. 4. (a) *P-E* hysteresis loop of the PSBZT ceramics. (b) Variation of P_r and E_c of the PSBZT ceramics.

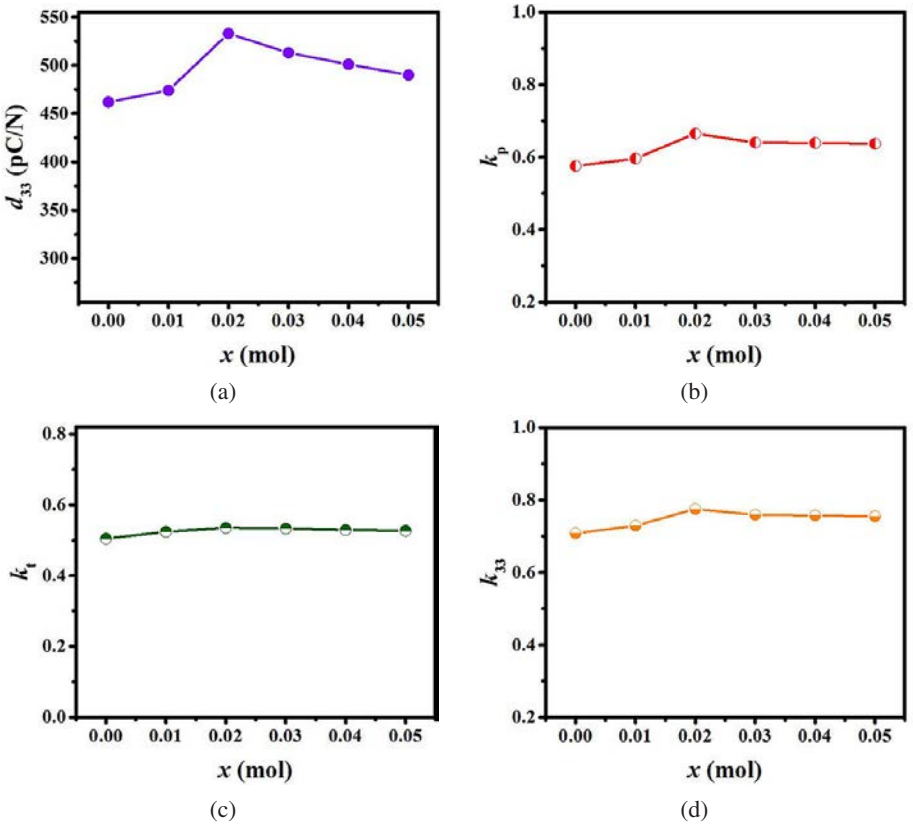

Fig. 5. (a) Variation of d_{33} for the PSBZT ceramics, (b) Variation of k_p of PSBZT ceramics, (c) Variation of k_t of PSBZT ceramics and (d) Variation of k_{33} of PSBZT ceramics.

of dielectric constant is much larger than the reduction of remnant polarization and electrostriction (Q_{33}) in the same system is considered constant, thus resulting in an increased piezoelectric charge coefficient in PSBZT ceramics. Figures 5(b)–5(d) display the variation of electromechanical coupling coefficient for the PSBZT ceramics including electromechanical coupling factors of planar mode (k_p), thickness mode (k_t) and longitudinal mode (k_{33}) which can be obtained based on the following formulas:

$$\frac{1}{k_p{}^2} = 0.398\frac{f_r}{f_a - f_r} + 0.579, \tag{2}$$

$$k_t{}^2 = \frac{\pi}{2}\frac{f_r}{f_a}\cot\left(\frac{\pi}{2}\frac{f_r}{f_a}\right), \tag{3}$$

$$(k_{33})^2 \approx (k_p)^2 + (k_t)^2 - (k_p)^2(k_t)^2, \tag{4}$$

where the f_r and f_a are resonant and anti-resonant frequencies.[13] It is clearly found that the k_p, k_t and k_{33} values gradually increase and then decrease with increasing Ba content, with the maxima values at the composition of $x = 0.02$, being on the order of 0.665, 0.535 and 0.775, respectively.

The temperature stability of ceramics is a critical parameter in determining their application environments. Here, we studied the annealing temperature dependence of the d_{33} for PSBZT system. To explore this temperature, the d_{33} values in the annealing temperature range of 25–400°C were measured at room temperature. Figure 6 depicts the effect of thermal annealing on the d_{33} of PSBZT system. The d_{33} values of all the samples decrease with the increasing temperature, while no significant change in d_{33} is observed for each sample at low temperature. It can be clearly observed that d_{33} is almost stable before 300°C for $PSB_{0.02}ZT$, indicating that the $PSB_{0.02}ZT$ ceramic has excellent thermal stability.

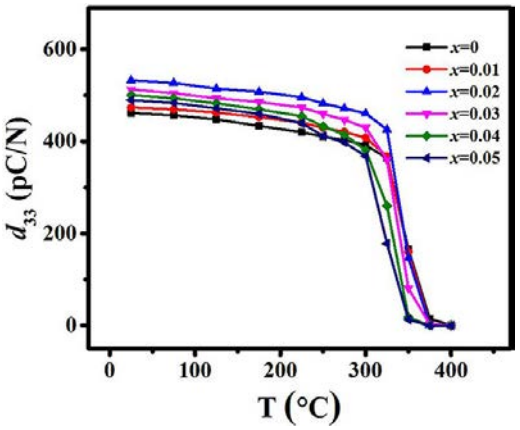

Fig. 6. Effect of thermal annealing on d_{33} of PSBZT ceramics.

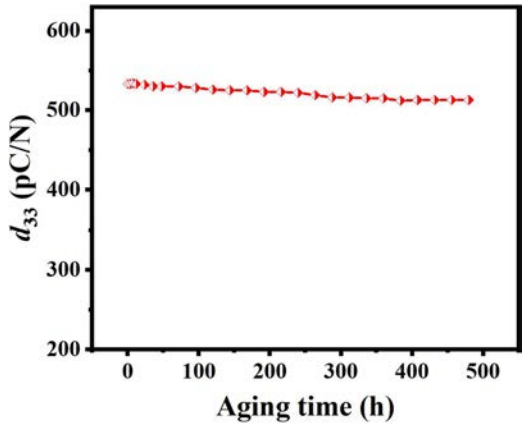

Fig. 7. The d_{33} $PSB_{0.02}ZT$ ceramic as a function of aging time at room temperature.

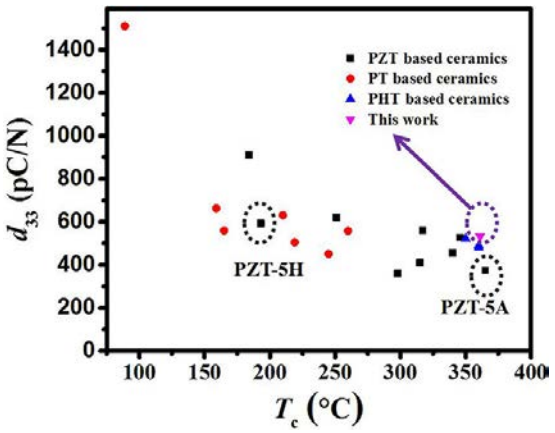

Fig. 8. Comparison of d_{33} and T_c of various Pb-based piezoceramics.

In practical applications, aging effect is a common occurrence in most ferroelectric materials, which significantly impacts the reliability of piezoelectric devices. Therefore, it is crucial to investigate the time-dependent piezoelectric properties of PSBZT. In this study, $PSB_{0.02}ZT$ ceramic was selected as a representative example. Figure 7 displays the d_{33} as a function of aging time at room temperature. It is evident that d_{33} decreases almost monotonically from 533 pC/N to 513 pC/N with increasing aging time. The decrease in d_{33} becomes progressively slower with increasing aging time and eventually stabilizes when the aging time reaches 480 h.

The comparison of d_{33} and T_c various Pb-based piezoceramics is shown in Fig. 8.[1,4–11,13,14,16,22,24–27] According to these data comparisons, it can be concluded that large d_{33} and high T_c are difficult to exist in a sample. It is noteworthy that the Curie temperature of $PSB_{0.02}ZT$ is higher close to 361°C. The T_c of PSBZT is higher than most lead-based piezoelectric ceramics, indicating that the sample is more suitable for broad temperature usage range. Compared with the current commercial PZT-5 ceramics, PSBZT ceramics show better temperature stability with similar piezoelectric performance.

The ultrasonic transducers were fabricated by using the prepared PSBZT and PSZT piezoelectric ceramics. Figure 9 depicts the structure schematic and images of the fabricated ultrasonic transducer. Table 2 displays the acoustic characteristics of the matching layer, piezoelectric substance and backing layer. The thickness of these structural parts of each transducer in this work is the same. The PSBZT and PSZT ceramic sheets were grounded to a thickness of 800 μm and the surface of sheets was cut to a diameter of 11 mm. Then, alumina powder with a particle size of 100 nm combined with epoxy (E-51) at a mass ratio of 1:1 is used to prepare the matching layer. To increase the bandwidth of the transducer, tungsten powder (5 μm) was gradually added to the epoxy at a mass ratio of 10:1. Air bubbles are subsequently eliminated from the backing while centrifugation compresses the tungsten particle distribution. A matching layer and a backing layer with the required thickness are attached to both sides of the piezoelectric ceramic sheet by an adhesive, then the copper wire was fixed and the transducer was enclosed.

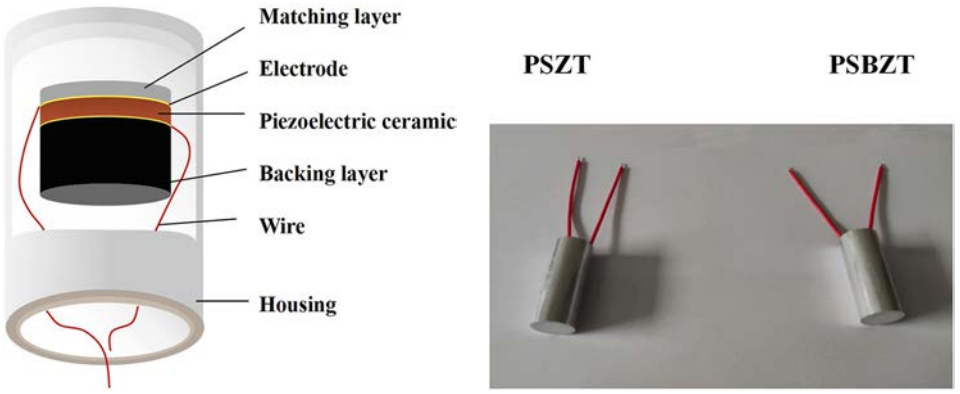

(a) (b)

Fig. 9. (a) Structure schematic of transducer and (b) Physical images of transducers for PSZT and PSBZT.

Table 2. Acoustic parameters of the matching layer, piezoelectric ceramic and backing layer.

	PSZT $x = 0$	PSBZT $x = 0.02$	Matching layer	Backing layer
Density ρ (g/cm^3)	7.45	7.5	1.874	6.591
Thickness (mm)	0.8	0.8	0.28	30
Diameter (mm)	11.0	11.0	13.0	13.0
Longitudinal Wave Velocity (m/s)	4408	4503	2801	1682
Acoustic impedance Z (MRayls)	32.8	33.7	5.2	11.1
Frequency constant Nt (kHz·mm)	1968	2092		

The pulse-echo response and FFT spectra of PSZT and PSBZT ceramics-based transducer are shown in Fig. 10. The center frequencies of all the transducers are around the 2.3 MHz. The PSZT ceramic-based transducer has a −6 dB bandwidth of 54.4% and an IL of −29.2 dB. While the PSBZT ceramic-based transducer has a −6 dB bandwidth of 61.3%

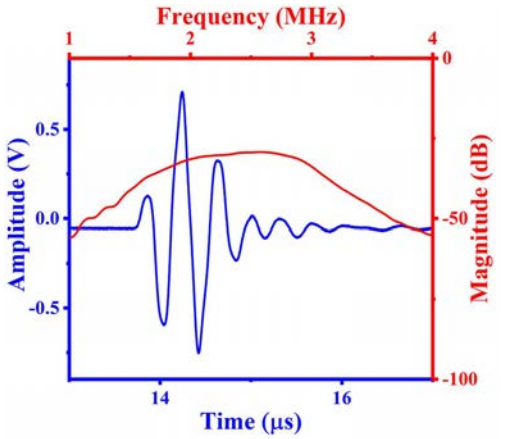

(a)

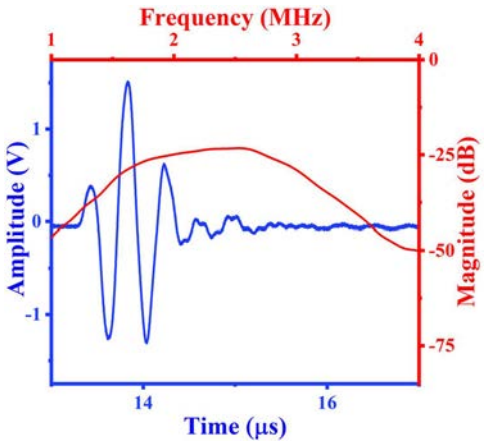

(b)

Fig. 10. Pulse-echo waveform and frequency spectra of the (a) PSZT ceramic transducer and (b) PSBZT ceramic transducer.

Table 3. Performance parameters of the transducers.

Transducer	Center frequency (MHz)	−6 dB bandwidth (%)	IL (dB)
PSZT	2.40	54.4	−29.3
PSBZT	2.31	61.3	−23.2

and an IL of −23.1 dB, the technical data of the transducers made from PSZT and PSBZT ceramics are listed in Table 3. The ultrasonic transducer prepared by PSBZT ceramic has higher sensitivity and bandwidth compared to the ultrasonic transducer prepared by PSZT ceramic, which is due to the larger d_{33} values and k_t values obtained in the PSBZT ceramics.

4. Conclusion

In this work, a series of $Pb_{0.99-x}Sm_{0.01}Ba_xZr_{0.53}Ti_{0.47}O_3$ ceramics were synthesized via a conventional solid-state method. In general, the effects of Ba^{2+} doping on the microstructure and electrical properties were investigated systematically. The results show that the doping of Ba^{2+} greatly improved piezoelectric performance of PSBZT due to the enhancement of dielectric permittivity. The PSBZT ceramics possess outstanding combination property (d_{33} = 533, pC/N, k_p = 0.665, T_c = 361°C, P_r = 38.97 μC/cm^2 and ε_r = 1850) when the content of Ba^{2+} was x = 0.02. Ceramic-based ultrasonic transducers were fabricated using PSZT and PSBZT ceramics and the performance of both was characterized and compared. It is shown that the IL of the PSBZT ceramic is much smaller compared to the PSZT ceramic-based transducer due to its larger piezoelectric coefficient. In addition, the bandwidth of the PSBZT ceramic sensor is improved due to the improved electromechanical coupling coefficient. It can be expected that PSBZT ceramic is an excellent candidate material for ultrasonic devices.

Acknowledgment

This work was financially supported by the National Natural Science Foundation of China (Grant Nos. 11404321, 52172085 and 51572056).

References

[1]G. H. Haertling, Ferroelectric ceramics: History and technology, *J. Am. Ceram. Soc.* **82**, 797 (1999).
[2]X. Qi, K. Li, L. Bian, E. Sun, L Zheng and R Zhang, Domain structure and dielectric diffusion-relaxation characteristics of ternary $Pb(In_{1/2}Nb_{1/2})O_3$-$Pb(Mg_{1/3}Nb_{2/3})O_3$-$PbTiO_3$ ceramics, *J. Adv. Dielect.* **12**, 2241002 (2022).
[3]L. Zheng, Y. Jing, X. Lu, S. Li, L. Yang, W. Lü and W. Cao, Temperature dependent piezoelectric anisotropy in tetragonal $0.63Pb(Mg_{1/3}Nb_{2/3})$-$0.37PbTiO_3$ single crystal, *Appl. Phys. Lett.* **113**, 102903 (2018).
[4]D. Wang, M. Cao and S. Zhang, Phase diagram and properties of $Pb(In_{1/2}Nb_{1/2})O_3$-$Pb(Mg_{1/3}Nb_{2/3})O_3$-$PbTiO_3$ polycrystalline ceramics, *J. Eur. Ceram. Soc.* **32**, 433 (2012).

[5]L. Ai, X. Li, Z. Wang, Y. Liu, C. He, T. Li, T. Chu, D. Pang, H. Tailor and X. Long, Preparation, structure, and electric properties of the $Pb(Zn_{1/3}Nb_{2/3})O_3$-$Pb(Yb_{1/2}Nb_{1/2})O_3$-$PbTiO_3$ ternary ferroelectric system ceramics near the morphotropic phase boundary, *J. Eur. Ceram. Soc.* **33**, 2155 (2013).

[6]Y. Hosono, Y. Yamashita, H. Sakamoto and N. Ichinose, Dielectric and piezoelectric properties of $Pb(In_{1/2}Nb_{1/2})O_3$-$Pb(Mg_{1/3}Nb_{2/3})O_3$-$PbTiO_3$ ternary ceramic materials near the morphotropic phase boundary, *Jpn. J. Appl. Phys.* **42**, 535 (2003).

[7]H. Tang, S. Zhang, Y. Feng, F. Li and T. R. Shrout, Piezoelectric property and strain behavior of $Pb(Yb_{0.5}Nb_{0.5})O_3$-$PbHfO_3$-$PbTiO_3$ polycrystalline ceramics, *J. Am. Ceram. Soc.* **96**, 2857 (2013).

[8]M. Zhu, P. Lu, Y. Hou, H. Wang and H. Yan, Effects of Fe_2O_3 addition on microstructure and piezoelectric properties of 0.2PZN-0.8PZT ceramics, *J. Mater. Res.* **20**, 2670 (2005).

[9]L. Zou, Z. Li, Z. Gao, F. Chen, W. Li, Y. Yu, Y. Li and P. Xiao, Microstructure and electric properties of Pr-doped $Pb(Zr_{0.52}Ti_{0.48})O_3$ ceramics, *Ceram. Int.* **47**, 19328 (2021).

[10]M. Zheng, Y. Hou, S. Wang, C. Duan, M. Zhu and H. Yan, Identification of substitution mechanism in group VIII metal oxides doped $Pb(Zn_{1/3}Nb_{2/3})O_3$-$PbZrO_3$-$PbTiO_3$ ceramics with high energy density and mechanical performance, *J. Am. Ceram. Soc.* **96**, 2486 (2013).

[11]R. Cao, G. Li, J. Zeng, S. Zhao, L. Zheng and Q. Yin, The piezoelectric and dielectric properties of $0.3Pb(Ni_{1/3}Nb_{2/3})O_3$-x$PbTiO_3$-(0.7-x)$PbZrO_3$ ferroelectric ceramics near the morphotropic phase boundary, *J. Am. Ceram. Soc.* **93**, 737 (2010).

[12]Y. Zhu, G. Jiang, Y. Li, Y. Liu, H. Zhang, S. Han, B. Yang, J. Liu and W. Cao, Temperature dependence of electrical and optical properties in Eu^{3+} doped $Pb(Mg_{1/3}Nb_{2/3})O_3$-$PbZrO_3$-$PbTiO_3$ ferroelectric ceramics, *J. Alloys Compd.* **897**, 163162 (2022).

[13]Q. Guo, F. Li, F. Xia, X. Gao, P. Wang, H. Hao, H. Sun, H. Liu and S. Zhang, High-performance Sm-doped $Pb(Mg_{1/3}Nb_{2/3})O_3$-$PbZrO_3$-$PbTiO_3$-based piezoceramics, *ACS Appl. Mater. Interfaces* **11**, 43359 (2019).

[14]J. Lin, B. Cui, J. Cheng, Q. Tan and J. Chen, Achieving both large transduction coefficient and high Curie temperature of Bi and Fe co-doped PZT piezoelectric ceramics, *Ceram. Int.* **49**, 474 (2023).

[15]K. Ramam and M. Lopez, Dielectric, ferroelectric and piezoelectric studies of neodymium-modified PLZNT ceramics for sensor and actuator applications, *J. Alloys Compd.* **466**, 398 (2008).

[16]F. Li, D. Lin, Z. Chen, Z. Cheng, J. Wang, C. Li, Z. Xu, Q. Huang, X. Liao, L. Chen, T. R. Shrout and S. Zhang, Ultrahigh piezoelectricity in ferroelectric ceramics by design, *Nat. Mater.* **17**, 349 (2018).

[17]S. B. Seshadri, M. M. Nolan, G. Tutuncu, J. S. Forrester, E. Sapper, G. Esteves, T. Granzow, P. A. Thomas, J. C. Nino, T. Rojac and J. L. Jones, Unexpectedly high piezoelectricity of Sm-doped lead zirconate titanate in the Curie point region, *Sci. Rep.* **8**, 4120 (2018).

[18]T. Ikeda, Studies on (Ba-Pb)(Ti-Zr)O_3 system, *J. Phys. Soc. Jpn.* **14**, 168 (1959).

[19]Z. Xu, X. Zeng, Z. Cao, L. Ling, P. Qiu and X. He, Effects of barium substitution on the optical and electrical properties of PLZT transparent electro-optical ceramics, *Ceram. Int.* **45**, 17890 (2019).

[20]L. Bian, K. Zhu, Q. Wang, J. Ma, J. Fan, X. Qi, G. Jiang, B. Zhao, R. Zhang, B. Yang and W. Cao, Performance enhancement of ultrasonic transducer made of textured PNN-PZT ceramic, *J. Adv. Dielect.* **12**, 2244003 (2022).

[21]D. Kang, K. L. Kim, D. G. Yang, Y. H. Jeong, C. Kim, J. Paik and H. Lee, Fabrication and testing of high performance acoustic emission sensor with Ta-doped lead zirconate titanate, *J. Electroceram.* **35**, 53 (2015).

[22]S. Huang, J. Zeng, L. Zheng, Z. Man, X. Ruan, X. Shi and G. Li, A novel piezoelectric ceramic with high Curie temperature and high piezoelectric coefficient, *Ceram. Int.* **46**, 6212 (2020).

[23]L. Jiang, H. Cheng, D. Sun, X. Zeng, L. Ling, P. Qiu and X. He, Effects of Ba^{2+} doping on microstructure and properties of PLMNT electro-optic ceramics fabricated by hot-pressed sintering process, *Ceram. Int.* **48**, 35259 (2022).

[24]S. Zhang, Z. Li, M. Zhang, D. Zhang and Y. Yan, Enhanced piezoelectric properties of PYN-PHT ceramics by LiF addition in low temperature sintering, *J. Alloys Compd.* **889**, 161649 (2021).

[25]S. W. Choi, T. R. Shrout, S. J. Jang and A. S. Bhalla, Dielectric and pyroelectric properties in the $Pb(Mg_{1/3}Nb_{2/3})O_3$-$PbTiO_3$ system, *Ferroelectrics* **100**, 29 (1989).

[26]V. Kalema, W. Y. Shihc and W. Shihb, Dielectric and piezoelectric properties of PMN-PT ceramics doped with strontium, *Ceram. Int.* **44**, 2835 (2018).

[27]D. Lin, Z. Li, F. Li, Z. Xu and X. Yao, Characterization and piezoelectric thermal stability of PIN-PMN-PT ternary ceramics near the morphotropic phase boundary, *J. Alloys Compd.* **489**, 115 (2010).